An Investigation of Tin Chalcogenide Precursors and Thin Film Materials for Applications in Energy Harvesting Devices

Ahmet, Ibrahim

Award date:
2017

Awarding institution:
University of Bath

Appendix B: Solid State Materials Characterisation (Theory and Procedures)

A.B.1 Scanning electron microscopy (SEM)

SEM is a common microscopy technique that can obtain information about a samples' surface morphology/topology, grain size, film thickness, and composition. The technique probes a specimen surface with a focused beam of high energy electrons (0.2 – 40 keV) with a spot size ranging between 0.4 to 5 nm in diameter and generated from a cathodic tungsten filament. Electrons dissipate into the sample producing a variety of emissions, which include ionizing secondary electrons, back scattered electrons and photons of various energies (X-rays, visible light, I.R. etc.). Subsequently the intensity of electron emissions are detected and used to constructs an image of the sample via a raster scanning pattern. Secondary electron imaging (SEI) is the standard detection mode used in an SEM and secondary electrons regularly emit close to the sample surface, which can be used to produce high resolution images, distinguishing details of ~1 nm in size and at x ~100,000 magnifications (depending on the instrument, the sample composition and its preparation). Often for surface imaging of uncoated semiconductors, a working voltage is between 5 to 10 keV is used and it is often lowered if the sample is being damaged by the electron beam or 'out-gassing'.[1]

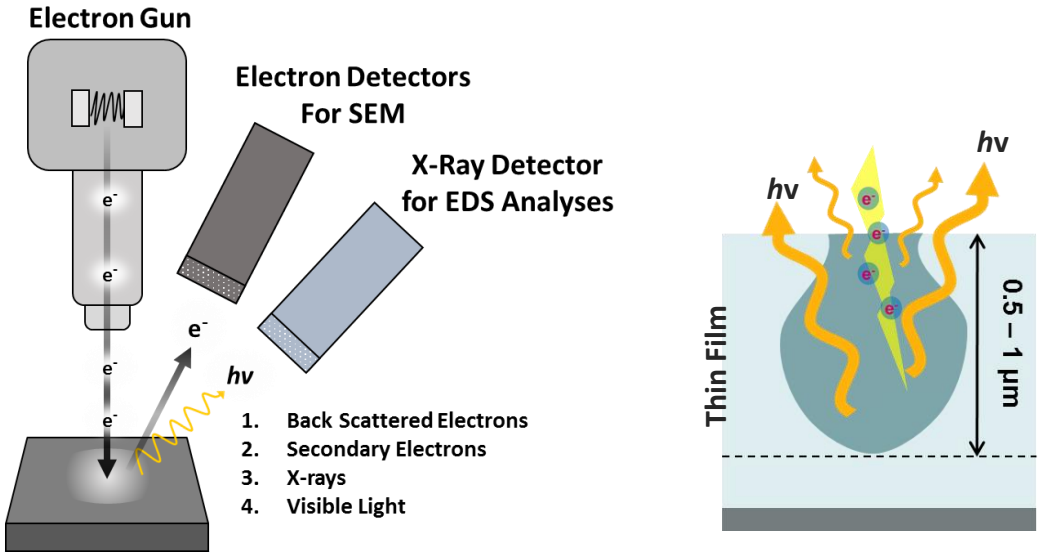

Figure B.37: (left) Basic design of an instrument for SEM imaging and EDS elemental analysis. (right) Spatial resolution of detected signal from EDS analysis.

A.B.2 Energy dispersive X-ray spectroscopy (EDS)

EDS is an analytical technique that qualitatively and quantitatively characterises the elemental composition of a sample in combination with SEM (or TEM) instruments. The technique realise on the removal of inner shell electrons from atoms within the sample surface, by bombardment with high energy electrons. Electrons in higher energy shells fill these vacant lower energy sites, correspondingly releasing energy in the form of X-rays emissions, which are then detected in accordance to frequency and intensity (no. of counts). The energies and intensities of the photon emissions are characteristic for specific atomic structures and can be indexed to qualitatively identify elements present within a sample. The intensity of a signals can be calibrated and used to estimate the relative quantities, such as weight %, of each elemental component within a specimen. However, the interaction volume of electrons can be relatively large (forming a tear drop shape that can extend between 100 nm to c.a. 5 µm into the specimen surface) and the X-rays generated have similar penetration depths. Therefore the data collected from EDS only presents an overall low resolution composition of sample. In most the signals from intrinsic and extrinsic surface carbon/ oxygen contaminates or the substrate and thin film sample or from multi layered thin film samples with different compositions are indistinguishable, even from spatial mapping techniques. Another limitation is that elements with $Z < 4$ i.e. H, He, Li and Be, cannot be detected and the detection limit of an SEM-EDS system is usually in the range of 0.1-0.5 wt %.[2]

A.B.3 X-ray photo emission spectroscopy (XPS)

The general mechanism and basic instrumental set-up for XPS is shown in **Figure B.38** X-rays (photons) of a specific energy (*hv* = 1,486.6 eV, 0.834 nm, Al Kα generally) are used to excite electronic states of atoms with the sample surface. Photoelectrons are ejected from the surface and travel via a hemi-spherical analyser (HAS), which filters them in terms of their kinetic energy (K.E.) before their intensity is recorded by a detector. Even though the X-ray penetrate deep into a sample, the inelastic mean free path (IMFP) of photoelectrons, which is the average distance an electron can travel through a solid before losing energy, is often in the range of ~10 nm for a ~1.4 keV X-ray source. Therefore, inelastic electron ejection contributes to the background signal rather than the well-defined primary photoelectric peaks.

The peaks generated in the spectra relate to the binding energy (B.E) of electronic states and core orbitals within atoms, and energies can be calculated using the following relation:

$$\mathrm{B.E.} = \mathrm{K.E.} - h\nu \qquad \textbf{(E.B.7)}$$

The spectra are presented in terms of binding energy (eV) against counts per second (CPS). Either a *survey* spectrum is generated from 0 to 1,400 eV or *high resolution* spectrum in the range of ~ 10-50 eV localised at specific electronic states of interest.

It is possible to differentiate between Sn 3p, 3d, 4s, 4p, 4d and valence electrons. By accurate determination of peak positions it is also possible to differentiate between atoms in different oxidation states or chemical environments, such as oxides and hydroxides. The XPS B.E. peaks represent the energies of electrons in their final states. These final states exist with sub-shells containing un-paired electrons due the removal of photoelectrons. Depending on the orbitals, a splitting of energy levels is observed in the final states and XPS doublet pairs exist in the spectra.

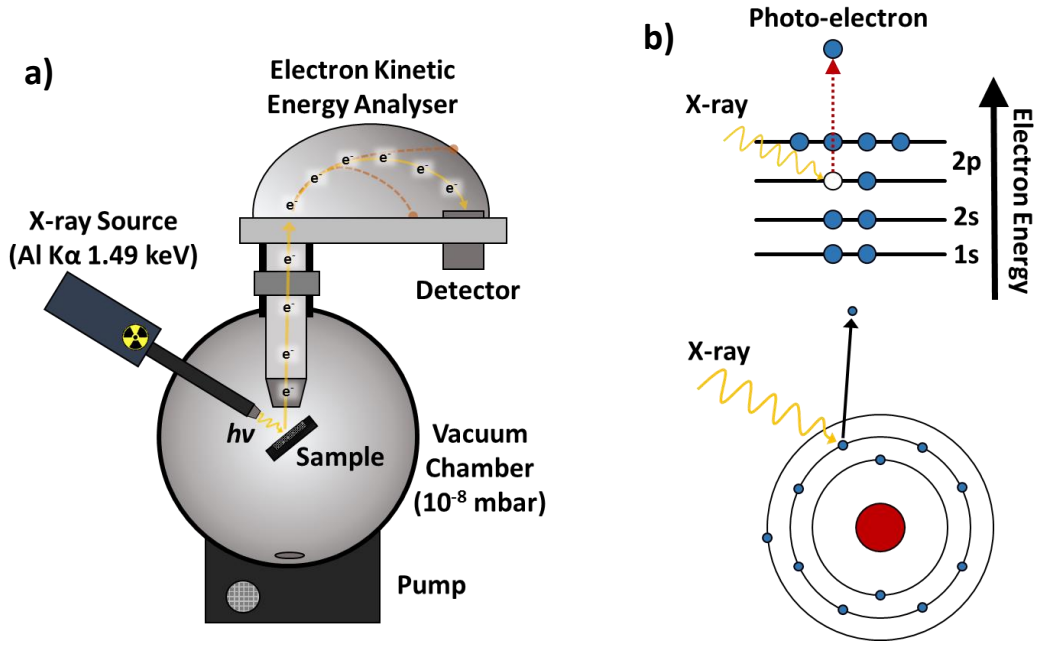

Figure B.38: a) Basic design of an XPS instruments. b) The principles of XPS relies on the photoelectron ejection from core electronic states by X-ray excitation.

Consequently, XPS is a powerful tool that can determine empirical formula, chemical states and electronic states on the surface of a material within a ~10 nm depth and in a parts per thousand range. Coupled with an ion beam etcher, depth profiling of a sample can also be achieved by analysing the surface between etches. The data can present changes in composition or chemical states throughout the film and the substrate beneath.

However, careful consideration must be taken when collecting, processing and interpreting raw data, many factors lead to inaccuracy, such as charging/ retarding fields from the sample, surface roughness, in-homogenous/non crystalline samples and orientation of the sample. Therefore some degree of prior knowledge about the sample is required.

There are many computations required to process and interpret raw XPS data which include:

- Removing background signal via a choice of algorithms.
- Accurate calibration of spectra and defining peak positions.
- Deconvolution of multiple over lapping peaks, which can arise from closely matched transitions. Subsequently produce synthetic peak models fitted to the data.
- Calculating the relative concentration of atoms and their chemical states, by determining relative area of fitted peaks.

Often there is some uncertainty in these processes and an accuracy of 10 % is typically quoted for a routinely performed XPS elemental concertation. [3]

A.B.4 Powder X-ray Diffraction (XRD)

XRD analysis is the most common practise of determining the crystallographic phase of a polycrystalline sample in materials chemistry.

The principle of XRD is that X-ray at a fixed wavelength (Cu Kα, 0.15418 nm) are generated and directed towards a sample at specific angles. X-rays can scatter off atoms which sit within planes of the Bravais lattice/s of crystallites in the sample and detected at the opposite incidence angle to the X-ray source. Using Braggs law (below), depending on the wavelength of X-rays (λ) and spacing between planes (d), coherent scattering is achieved at specific angles (α) and detected at higher counts compared to the background detection.

$$2\mathrm{d}\sin\theta = n\lambda \quad \textbf{(A.1.8)}$$

Diffraction pattern is generated by analysing a sample at multiple angles and the data is presented in terms of 2θ vs X-ray intensity. Peaks can be allocated to a specific miller indices of the crystallographic systems within the sample.[4] The high penetration depth of X-rays can often result in the generation of diffraction peaks from both the thin film sample and underlying substrate. Broad or no diffraction patterns are detected if the sample is made up of microcrystalline or amorphous material. Indexed diffraction files from databases, such as the ICDD, can be used to identify peaks in a spectrum using software such as Diffrac.suite™, to process raw data and statistically confirm matched spectra.

XRD analyses can be used to determine the phase purity, crystallinity, grain size and preferential lattice orientation of polycrystalline thin film samples.

A.B.5 Atomic force microscopy (AFM)

AFM is used to measure the localised surface topology, thickness and friction of a sample. There are many varieties of AFM modes, but the principle analytical techniques is achieved by contacting a sample surface with a mechanical probe known as an apex and scanning across the surface of a samples and measuring the difference in x,y and z co-ordinates as the sample surface applies a force on the probe tip. Resolution on the order of 0.1-1 nm can be achieve. The technique is useful for comparing thin film samples in terms of crystallite size and dimension. Likewise surface roughness values, such as the root mean square (RMS), can be calculated and used to assess the quality and viability of thin films for device fabrication. It is often ideal for thin films to be smooth allowing for the uniform deposition of subsequent thin film layers. AFM is also used to measure film thicknesses by removal of thin films from the substrate the AFM probe can be scanned across the film edge and measure the difference in height between the film and substrate at multiple regions.[5]

A.B.6 Raman Spectroscopy

Raman analyses is a type of vibronic spectroscopy that can be easily and quickly used to qualitatively characterise a material surface and bulk composition at a micron scale (if the samples are Raman active).

Raman analyses relies on the inelastic scattering of monochromatic light from a material surface. The molecule structure is irradiated with a photon of known energy this distorts (polarizes) the cloud of electrons within the molecular bond and causes an excitation from the vibrational ground state (v^0) to form unstable higher energy vibrational states called a 'virtual state'. For a Raman scattering process the molecule relaxes into a different rotational or vibrational 'final state' (rotovibronic state) at a different energy levels than the starting vibrational state. For this to occur the incidence photon interacts with vibrational modes with cause a change in polarizability in the structure, unlike IR spectroscopy, where the incidence photon interacts with vibrational modes that cause a change in the permanent dipole moment. This inelastic interaction causes the photon released from the transition from the virtual to final state to be either be, of discrete lower energies (Stokes shift) or higher energies (anti-Stokes Shift) compared to that of the incidence photon. During analyses Raman scattered photons emitted from the sample are collected through a lens and separated from other elastic Rayleigh scattered radiation and then detected. The Raman spectrum is commonly presented in CPS vs. Raman shift in units of wavenumbers (cm^{-1}), which the difference in energy (ΔE) from the incidence signal.

Peaks in the spectrum correspond to energy difference of Raman active vibrational states that are often on the scale of 100 to 3000 cm^{-1}. The intensity of Raman signal is directly proportional to the laser photon flux. However, using focused high power lasers can cause thermal damage to a sample. This may be useful as one may capture Raman spectra during thermal treatment of the sample and monitor its effects.

The number, position and intensities of Raman peak are sensitive to the materials phase, polymorph and solid form (crystallite size or morphology) as well as composition, since the number of Raman active transition and energies of vibrational states depend of the arrangement of atoms in space. Even when a material has identical formulae, but different crystal structure or phase it will result in distinctively different spectra. Therefore Raman can be useful for assessing the purity of samples and clearly distinguish between multiphasic systems. A large variety of materials and pure crystals have been characterised via Raman spectroscopy, and this technique can be used to identify which materials are present in a sample. Interestingly, peak positions may change slightly in energy when comparing spectra of pure crystals and samples. This can reveal information about stoichiometries or size of the crystallites in the specimen.[6,7]

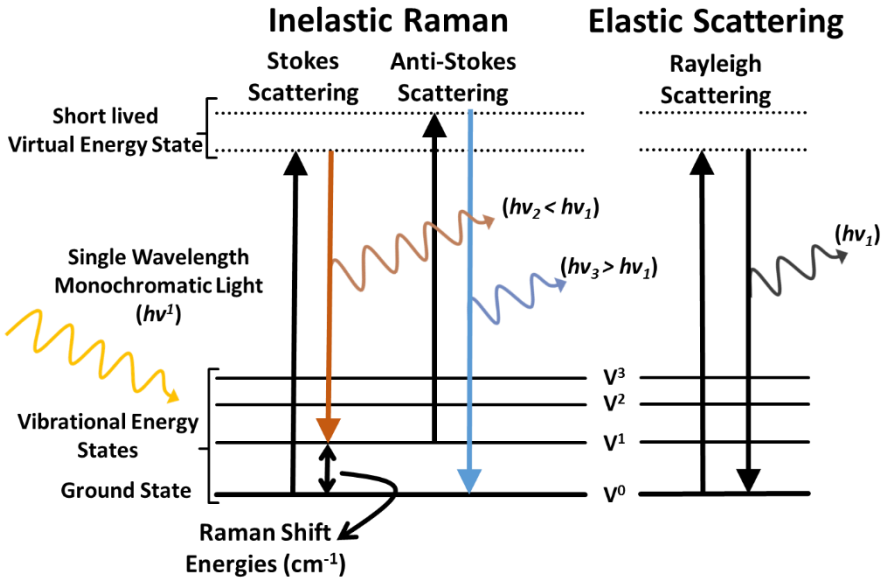

Figure B.39: Raman scattering processes.

List of Referenced Raman Peaks

Table B.1: List of referenced Raman peaks at an excitation wavelength of 532 nm.

Material	Symmetry	Raman Shift	Relative Intensity	Reference
SnO	B_{1g}	109 cm^{-1}	1	(8)
	A_{1g}	209 cm^{-1}	~1	
SnO_2	B_{1g}	87 cm^{-1}	<0.01	(9)
	E_g	472 cm^{-1}	<0.01	
	A_{1g}	632 cm^{-1}	1	
	B_{2g}	773 cm^{-1}	0.25	
α-SnS	B_{1g}	68 cm^{-1}	0.1	(10)
	A_g	96 cm^{-1}	1	
	B_{3g}	163 cm^{-1}	~0.7	
	B_{2g}	191 cm^{-1}	~0.9	
	A_g	219 cm^{-1}	~0.4	
	B_{2g}	286 cm^{-1}	<0.1	
Cubic-SnS	-	71cm^{-1}	0.9	(11, 12)
	-	90 cm^{-1}	0.95	
	-	111 cm^{-1}	0.95	
	-	173 cm^{-1}	1	
	-	192 cm^{-1}	0.5	
	-	204 cm^{-1}	0.85	
	-	230 cm^{-1}	<0.1	
	-	262 cm^{-1}	<0.1	
Sn_2S_3	-	88 cm^{-1}	0.1	(13)
	-	185 cm^{-1}	<0.1	
	-	235 cm^{-1}	0.25	
	-	252 cm^{-1}	0.15	
	-	302 cm^{-1}	1	
SnS_2	E_g	205cm^{-1}	<0.1	(13, 14)
	A_{1g}	314 cm^{-1}	1	

Table B.2: List referenced Raman peaks at an excitation wavelength of 532 nm.

Material	Symmetry	Raman Shift	Relative Intensity	Reference
α-SnSe	A_g	75 cm^{-1}	0.8	(10)
	B_{3g}	110 cm^{-1}	1	
	A_g	133 cm^{-1}	0.75	
	A_g	154 cm^{-1}	0.6	
Cubic-SnSe	-	69 cm^{-1}	1	(15)
	-	156 cm^{-1}	0.4	
	-	185 cm^{-1}	0.5	
$SnSe_2$	E_g	116 cm^{-1}	<0.1	(14)
	A_{1g}	186 cm^{-1}	1	
SnTe	-	-	-	-
Te	-	92 cm^{-1}	<0.1	(16)
	-	123 cm^{-1}	1	
	-	140 cm^{-1}	0.1	
Graphene	D peak	1350 cm^{-1}	0-1	(17)
	G peak/E_{2g}	1580 cm^{-1}	0.25	
	G' peak/$2D_{Band}$	2676 cm^{-1}	1	
Graphene	D peak	1350 cm^{-1}	0-1	(17)
	G peak/E_{2g}	1580 cm^{-1}	0.25 to >1	
	G' peak/$2D_{Band}$	2676 cm^{-1}	1	

A.B.7 Photoluminescence excitation

Photoluminescence (PL) excitation spectroscopy examines the interaction of photons with charge carriers within a material and particularly useful for analysing and assessing the properties and quality of a semiconductor samples especially for photovoltaic applications. This technique exposes a semiconductor sample to an excitation light source at a specific wavelength often at photon energies in excess of the semiconductor band gap. Photons of a high energy are absorbed by the semiconductor and a photo- electron hole pair are generated. The photo generated electrons reach an excited state, then relaxes via transferring between intermediate lower energy states via non radiative processes. At energy levels close to the conduction band edge photo-electrons will transfer back to the ground state via a number of possible radiative processes resulting in an electron-hole recombination and a photon-emission at wavelengths greater than the excitation wavelength. At room temperature there is a broad emission spectrum generated due to the combination of probable radiative transitions at various energies following a Boltzmann distribution.

A PL spectrum present the detected emission frequency or wavelengths against intensity. All peaks in a PL spectrum refers to a recombination process. The highest intensity peaks often correspond to the main recombination centre and generally corresponds to direct or indirect optical band gap energies of the semiconductor. However, other peaks in PL spectrum can relate to other recombination processes. Often emission peaks of low energies can correspond to traps states within the band gap. Thus PL spectroscopy can be useful for assessing the quality of samples for optoelectronic applications, as well as, qualitatively determining the presence of a semiconductor material.[18]

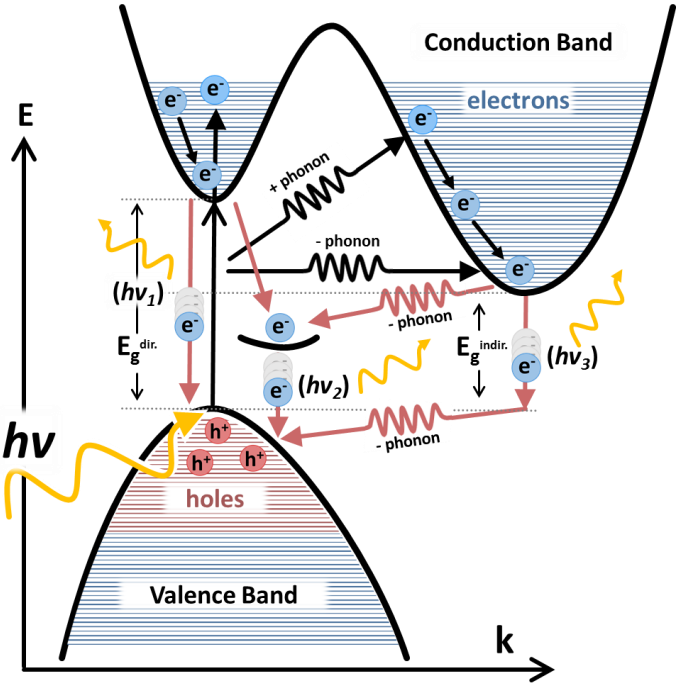

Figure B.40: Illustration of photoelectron generation mechanism and the photoluminescence processes (hv_1, hv_2 [trap assisted], hv_3) in an indirect band gap semiconductor.

A.B.8 Solid state UV-Vis-IR spectroscopy (SS-UV-Vis-IR)

A SS-UV-Vis-IR spectrometer can record the intensity of transmitted, absorbed, and reflect light at a range of wavelengths. Principally absorption spectroscopy is complimentary to PL and measures the extent of electron transitions from ground state to excited states as light passes through a sample. For a thin film semiconductor sample, transmission and reflectance data as a function of photon energies can be used to obtain information such as optical band gap energies, refraction index, absorption coefficients, film thicknesses and propagation constants. Semiconductors show an increased absorption at photon energies close to the band gap energy, known as the absorption edges, since photo generated electrons begin to possess sufficient energy to transition across the band gap. This feature of an absorption spectrum can be used to determine optical band gaps of samples.

Absorption Coefficient, Tauc's Relation and Band Gap Energy from UV-Vis-IR Transmittance and Reflectance Spectroscopy.

It is important to calculate the absorption coefficient (α) of a semiconductor in order to derive the band gap (Eg) of the material. By measuring a material's absorbance spectrum the absorption coefficient can be calculated at different wavelengths (nm or *hv*) using the following relation (Beer-Lamberts Law):

$$\mathrm{I} = \mathrm{I}_0 e^{-\alpha \mathrm{d}} \quad \textbf{(E.B.9)}$$

Where $\mathbf{I}$ is the detected light intensity, $\mathbf{I_0}$ is the source light intensity, $\mathbf{d}$ is the film thickness and $\boldsymbol{\alpha}$ is the absorption coefficient of the film. By rearranging the equation and converting to common logarithm the following expression for the absorption coefficient can be generated:

$$\alpha = 2.303.\mathrm{Log}\left({}^{1}/_{T}\right).\left({}^{1}/_{d}\right) \quad \textbf{(E.B.10)}$$

Where $\mathbf{T}$ is the transmittance at a given wavelength ($\mathbf{T} = \mathbf{I}/\mathbf{I_0}$ x 100). Using the equation above we can determine the absorption coefficients for of the thin films deposited from transmittance (%) data and a set film thickness (nm). The film thickness can be calculated via a number of routes. From a uniform thin film semiconductor sample one could adopt the 'envelope method'; from transmittance and absorbance spectroscopy, interference maxima and minima can be visualised at wavelengths lower than bandgap energy (*hv* < Eg) of thin film

sample. The envelope curves $T_{max}(\lambda)$ and $T_{min}(\lambda)$ can be obtained firstly by a free hand drawn extrapolation of the maxima and minima points of the interference fringes. Then the extrapolated curve can be digitized to form a parabolic fit of $T_{max}(\lambda)$ and $T_{min}(\lambda$, shown in **Figure B.41**.[19-21]

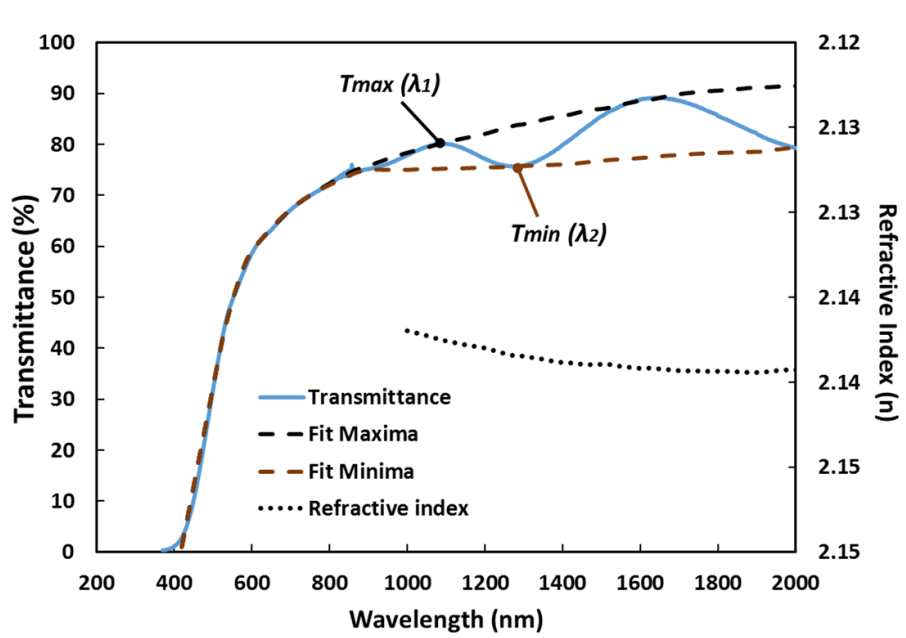

Figure B.41: An example of the transmittance spectrum with inference peaks and calculated Refractive index (n) for a ~550 nm SnS_2 thin film sample deposited on a glass substrate, with a direct band gap of ~1.27 eV.

From this one can determine the refractive index of the films deposited (n) if the refractive index of the substrate is known (n_s) using the following relations:

$$n = [\mathrm{N}' + (\mathrm{N}'^2 - n_s)^{0.5}]^{0.5} \quad \textbf{(E.B.11)}$$

Where,

$$\mathrm{N}' = 0.5\,(n_0 + n_s^2) + [2n_s \left[\frac{T_{max} - T_{min}}{T_{max}T_{min}}\right]] \quad \textbf{(E.B.12)}$$

Where $\mathbf{T_{max}}$ and $\mathbf{T_{min}}$ are the wavelength (**λ**) dependant envelope functions and $\mathbf{n_o}$ is the refractive index of air, which is equal to 1.The value used for refractive index of the substrate ($\mathbf{n_s}$) and can either be n_s = 1.52 when films are deposited onto glass or $\mathbf{n_s}$ = 2.00 for TEC 7 Fluorine Doped Tin Oxide (FTO) substrates. These are the averaged refractive index values of the given substrates at wavelength between 800 – 2000 nm.

Knowing the refractive index for the films at wavelengths for the maxima and minima of the interference pattern, the following equation can be then used to calculate the film thickness:

$$d = \frac{\lambda_1 \lambda_2}{2[n(\lambda_1)\lambda_2 - n(\lambda_2)\lambda_1]} \quad \textbf{(E.B.13)}$$

Where **n(λ_1)** and **n(λ_2)** are the refractive indices at two adjacent maxima (or minima) at **λ_1** and **λ_2**. Various **d** values can be calculated from the recorded spectrum and can be averaged to determine an accurate film thickness (nm).

However this approach can only be adopted when thin film samples are smooth and uniform. In these cases when no sinusoidal interference spectra is observed one can determine the film thickness from step off AFM or cross section SEM and both pieces of data (if sufficient) can be used to estimate the average film thickness of a sample.

With the film thicknesses determined, using equation **1.13**, the wavelength dependant absorption coefficient (α) can be calculated. One can then use the Tauc relation (below) to determine optical band gaps in semiconductor thin films.

$$\alpha h\nu = B(h\nu - E_{\mathrm{g}})^{Y} \quad \textbf{(E.B.14)}$$

Where E_{g} is the optical band gap, ***h*** is the Plank's constant, ***v*** the frequency of incidents photons, ***B*** is a constant called the band tailing parameter, and ***Y*** is the index for transition types, which can have different values (2, 3, ½ amd 1/3) corresponding to the indirect allowed, indirect forbidden, direct allowed and direct forbidden transitions, respectively. The band gaps of the deposited films can then be determined by plotting $(\alpha h\nu)^n$ vs. $h\nu$ and extrapolating the linear region of the plot to the axis and close to the onset absorption edge. Where the linear extrapolation insects the x-axis, (when $(\alpha h\nu)^n = 0$) the x-axis (eV) value corresponds to the respective band gap transition energy (direct for $Y = ½$ and indirect for $Y=2$).[22]

A.B.9 Photoelectrochemical Analysis

This investigation will be concerned with the opto-electronic properties of some semiconducting thin film samples, including SnS_2, α-SnS and cubic-SnS. It is important to assess these properties of the sample as it can present a greater insight into the semiconductor properties as well as an understanding of the stability and quality of samples and determining their viability for use in optoelectron devices, such as solar cells.

In order to determine these properties, electrical contacts must be made with the photo-absorber/ semiconductor layer while the surface is simultaneously illuminated. A convenient method is to carry out photoelectrochemical measurements of the samples. For this a thin film must be deposited onto conductive substrates (i.e. FTO, Graphene or Mo) and immersed in transparent conductive electrolyte solution containing an appropriate redox active species. The redox species should be efficient at collecting photo-generated minority charge carriers from the film surface, so that these carriers do not induce photo corrosion of the film. If this is achieved the semiconductor-electrolyte interface is non-damaging, reproducible and easily set-up compared to a solid state junction. It will be appropriated that the relevant theory that governs different types of photoelectrochemical measurements and the processes at the semiconductor-electrolyte junction to be presented in this section. For further reading of 'The semiconductor-electrolyte interface' by W. Schmickler and E. Santo is recommended.[23]

Throughout this section n-type SnS_2 thin film semiconductors will be used to illustrate the various processes at the semiconductor-electrolyte junction, but the same theory can be adapted to other materials studied in this PhD, which include thin film samples of p-type α-SnS and ambi-polar cubic-SnS.

n-type SnS_2

As discussed previously, SnS_2 is a relatively wide band gap semiconductor (E_g = 2.4 to 2.9), and is extrinsically n-type with a carrier concentration of about 10^{17} to 10^{18} cm^{-3}.[24-26] An n-type semiconductor like SnS_2 contains a number of 'charge carriers'. These form as a result of off-stoichiometries, impurities or defects, such as sulphur vacancies, which contribute excess free negative charge carriers (electrons) that occupy allowed states close to the conduction band (CB) minimum. Free electrons are termed as the 'majority carrier' in an n-type material and originate from 'donor impurities'. In contrast the existence of positive charge carriers (electron holes) is dramatically less and are known as 'minority carriers'. For the purpose of this investigation, it is considered that electron holes do not diffuse (conduct) through n-type semiconductors and electrons do not transport through p-type materials and in both cases they are subject to high resistivity, as a result of a small diffusion lengths (<1 µm).

Semiconductor-electrolyte Interface

SnS2 is an n-type semiconductor and will therefore have the Fermi level close to the CB edge. The Fermi level is effectively equivalent to the electrochemical potential of the negative majority carriers within the material. When an n-type material is immersed in a solution containing a redox species with a redox potential between the conduction and valence band energies and below the Fermi level, charge transfer occurs from the semiconductor to the redox species (Figure 1.42). Electrons (majority carriers in an n-type material) will lower their energy by transferring from the semiconductor surface and reduce the redox electrolyte. The loss of electrons creates positively ionised donor sites at the interface, which causes further electron diffusion from the bulk to the interface to compensate for the generation of ionised donor sites. This generates a region close to the semiconductor-electrolyte interface that is depleted of charge carriers. It is known as the 'space charge' or 'depletion' region, extending a depth W into the semiconductor. The loss of electrons from the bulk causes the Fermi level, conduction and valence bands to lower in energy. Furthermore due to the transfer of negative charge carriers to the space charge region the conduction and valence bands in this region do not decrease as the Fermi level lowers, and a 'band bending' phenomena occurs. As a result an electric field is generated at the surface and is equivalent to the degree of band bending $\Delta\phi$ over the depth of the space charge region, W. Furthermore the space charge region generates a rectifying contact with the electrolytes, known as a Schottky barrier and providing a driving force for the separation of photo-generated electron-hole pairs. In addition to the space charge region, a thin plane (c.a. 3-5 Å) known as the Helmholtz layer, is formed from absorbed ions onto the semiconductor surfaces and has a small influence on the overall potential of the system. The Fermi level will continue to lower until it matches the redox potential of the electrolyte and reaches equilibrium.

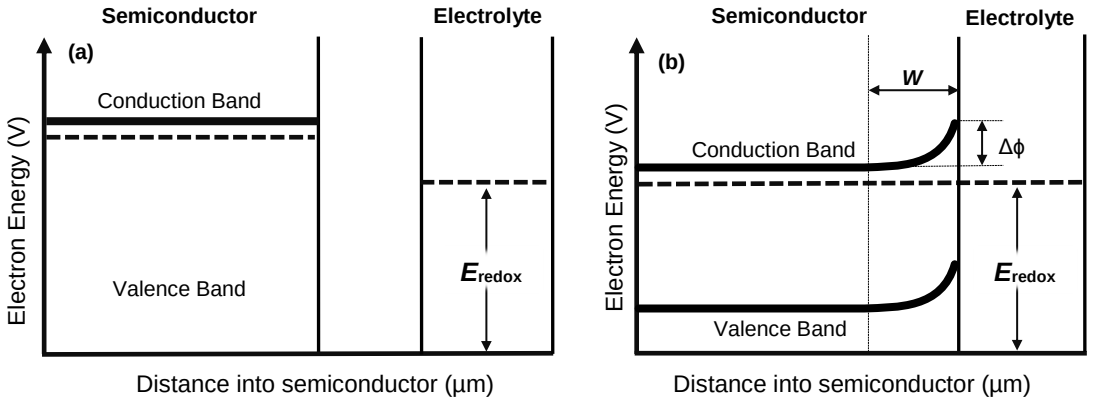

Figure B.42: (a) Energy levels in a semiconductor (left-hand side) and a redox electrolyte (right-hand side), shown on an energy scale for a common vacuum reference scale. (b) The n-type semiconductor-electrolyte interface when the two phases are in contact and have reached equilibrium.

Fermi-level Control

The depth, *W*, of the space charge region and extent of band bending, Δϕ, is important for our investigation. The electrochemical system used, to investigate the photo-electrochemical response of the n-SnS_2 films, was made up of a 0.1 M sodium sulphite (Na_2SO_3) aqueous electrolyte at c.a. pH 7. The oxidation of sodium sulphite is known to be electrolytically irreversible, and oxidises to either to sodium sulphite (Na_2SO_4), at -1.156 V or to sodium dithionate ($Na_2S_2O_6$), at -0.183 V vs. Ag|AgCl. It is therefore an efficient hole scavenger suitable for removing minority carriers from an n-type semiconductor interface. (Note: for the analyses of p-type semiconductors, such as SnS, an $Eu^{2+/3+}$ redox species is used instead, since it is an effective and reversible scavenger of electron minority carriers)

In addition our electrochemical cell consisted of three electrodes; a platinum counter electrode, an Ag|AgCl reference electrode and the sample as our working electrode (please refer to experimental Section…….). As described above, when the sample is initially immersed into the electrolyte the equilibrium process between the semiconductor-electrolyte redox couple will occur. However, during measurements the sample is connected to a potentiostat. This will control the potential, *E*, of the sample with respect to an Ag|AgCl reference electrode. By controlling the potential we are adjusting the position of the Fermi level within the semiconductor. By controlling the Fermi level of the semiconductor we can adjust the amount of charge exchange at the semiconductor-electrolyte interface. Furthermore the depth of the space charge region, *W*, and the degree of band bending Δϕ can be adjusted. At a specific potentials (or Fermi level energies) the space charge region can

equal zero and this is known as the 'flat band' potential, E_{fb}, and can give you an understanding of the relative electrochemical potential of your material. When the carrier concentration of your semiconductor is less than c.a. 10^{18} cm^{-3}, most of the potential is controlled across the space charge region, with a small potential drop across the Hemholtz layer.

For this case we can say the degree of band bending equals the difference between the flat band potential and applied potential ($\Delta\phi = E_{fb} - E$). Therefore the applied potential, E, can be related to the depth of space charge region, W , given by Gärtner equation:

$$W = \left(\frac{2\varepsilon_0\varepsilon_r(E_{fb} - E)^{\frac{1}{2}}}{qN_{ald}}\right) \quad \textbf{(E.B.15)}$$

Where ε_0 is the vacuum permittivity, 8.85×10^{-12} Fm^{-1} and ε_r the relative material permittivity approximated as 10, q is the electron charge density (1.602×10^{-19} C) and N_d is the donor concentration for an n-type semiconductor, such as SnS_2, and N_a is the acceptor concentration for a p-type semiconductor, such as ortho-SnS (c.a. 4×10^{17} cm^{-3}).

Figure B.43 illustrates how varying the applied potentials across the SnS_2 thin film in the electrolyte solution can change the degree of band bending and the size of the space charge region at the semiconductor-electrolyte interface. In Figure 1.43 b we see that under a small positive bias relative to the flat band potential, a small space charge region is generated. With an increasing positive bias (see Figure 1.43 d) the degree of band bending ($\Delta\phi$) increases and a larger space charge region is generated. The electric field over the space charge region provides a driving force for holes to move to the surface and energy barrier for electrons causing them to move away from the surface and into the bulk of the film. At a negative bias potential the Fermi level is raised and the electric field over the space charge region provides an opposite driving force for electrons to move to the surface and hole migration into the bulk (**Figure B.43 c**).

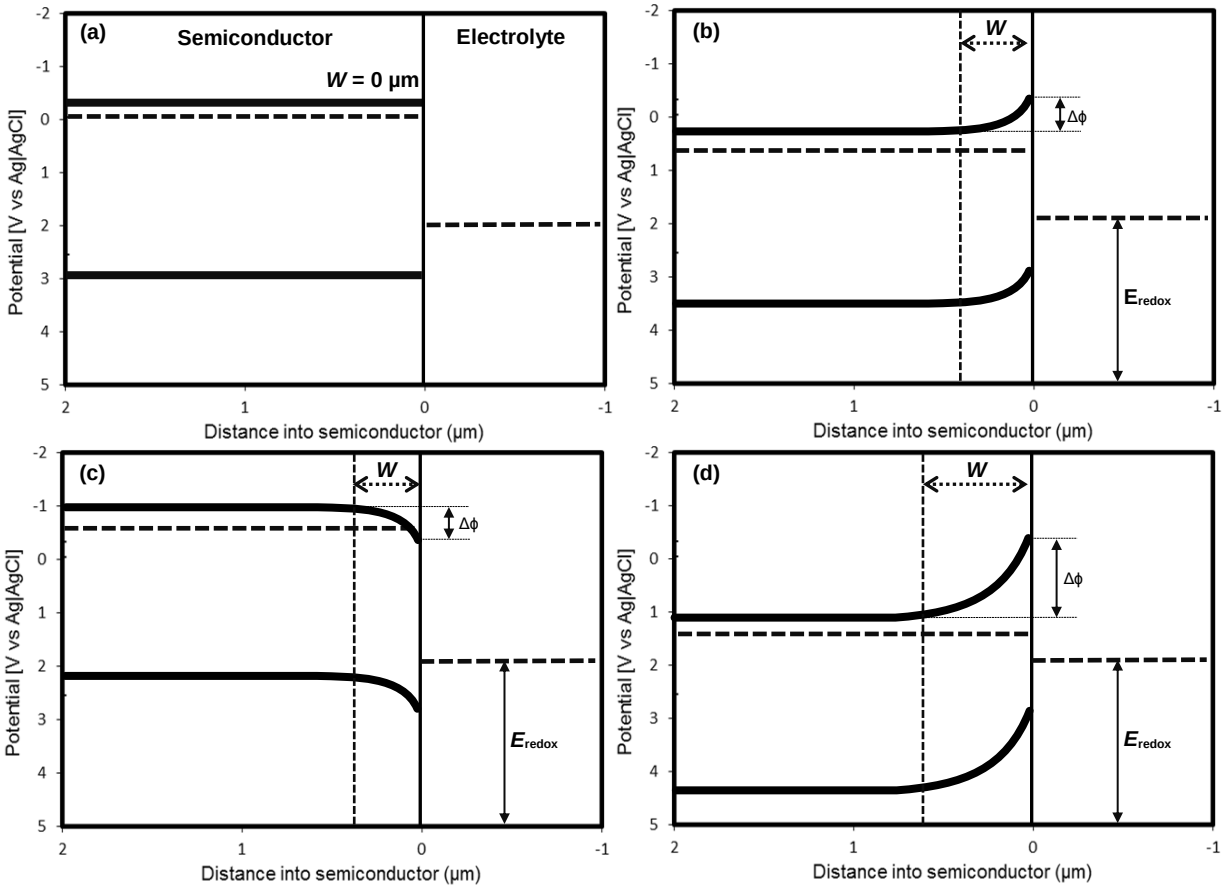

Figure B.43: SnS_2 n-type semiconductor-electrolyte interface under different applied potential, *E*, with respect to the Ag|AgCl reference electrode: (a) -0.047 V, flat band potential for this example (W=0), (b) + 0.75 V (W=0.47 µm), (c) -0.75 V (W=0.44 µm) and (d) + 1.2 V (0.59 µm).

For photo-current to be generated under illumination, the photo excited electrons and holes must initially separate and propagate in opposite directions. The electric field generated at the semiconductor/electrolyte, when $\Delta\phi \neq 0$, provides the necessary driving force for separation. As seen above when a semiconductor is subject to a negative bias, relative to the flat band potential, photo generated electrons will move to the surface and holes will diffuse into the bulk. For a n-type semiconductor, where holes are minority carriers, under a negative bias potential, you would expect minimal or zero photocurrent generation, since holes will only travel as far as the minority carrier diffusion length (L_n) resulting in high recombination rate or holes terminating in trapped states. However, under a positive bias, the semiconductor-electrolyte junction provides an electric field, over the space charge region, for electrons to move into the bulk of the film and holes to migrate to the surface. Together with this, the effective reducing electrolyte ($NaSO_3$) can rapidly remove holes from the surface

and the rate of electron collection from the semiconductor surface is negligible. Furthermore an n-type semiconductor, such as SnS_2 will effectively conduct the photo generated electrons to the back contact with minimal resistance. Subsequently a large photo current should be observed for an n-type semiconductor under positive bias. (This will be the opposite case for a p-type semiconductor).

Being able to control the degree of band bending and the distance of the space charge region can also have an effect on the amount of photo current generated. If there isn't recombination at the semiconductor-electrolyte interface, all photons absorbed within the space charge region will generate photo current, since there is effective electron-hole separation. Photons absorbed further than the space charge region will generate excited electron-hole pairs, however, minority carriers (holes) will only be collected, at the electrolyte interface, if they can diffuse far enough to reach the space charge region. This process is dependent on the minority carrier diffusion length (L_n). The processes that are involved in the absorption of photons and generation of photocurrent can be summarised in the Gärtner equation to give an expression for the 'external quantum efficiency' (EQE):

$$\phi(E) = 1 - \frac{\exp(-\alpha(E)W)}{1 + \alpha(E)L_n} \quad \textbf{(E.B.16)}$$

Where α(E) is the photon energy dependant absorption coefficient of the semiconductor. When the material is subjected to a photon energy at which the absorption coefficient is relatively high and irrespective of a material with a small minority carrier diffusion length (<0.1 µm), increasing the space charge region (W), will increase the photon-current or EQE generated at these photon energies. This is because a larger number of photons will be absorbed within the space charge region and generate excited electron-hole pairs that will separate well under the force of an electric field (**Figure B.44**).

Conclusively the importance of the applied potential has been established, since it can be used to control the Fermi level of the semiconductor sample and the degree of band bending at the semiconductor–electrolyte interface. Subsequently the depth of the space charge region can be selected, so that the majority of the light is absorbed in this region and the sample will generate as much photo-current possible. However, there is a limitation to the depth of the space charge region. If potentials are brought too negative or positive of the flat band

potential, electrochemical processes such as hydrogen generation or oxidation of the sample surface can occur, which can result in the degradation of the sample which can enhance surface recombination. Furthermore if the sample consist of pinholes a large dark currents will be observed and will increase with increasing potentials. This can shadow the photocurrent generated from chopped illumination and photo current will become undetected at high potentials. Therefore sample are kept within potential range of -1 to +1 V vs Ag|AgCl reference electrode. No current should be detected when the sample is not illuminated for an ideal sample.

Photoelectrochemical Responses under Chopped Illumination

To measure the effects of potential or change in band bend has on photo-current generation, a sample is subjected to a chopped illumination at a fixed wavelength, whilst subjected to a sweeping potential from negative to positive. Photo-currents are distinguishable from dark currents by the sudden switching between high and low current densities. If a persistent photocurrent decay is observed after illumination is terminated, this can indicate that the sample contains trap states within the band gap.

Measuring the quantum efficiency spectra

Now that we have discussed the importance of the semiconductor-electrolyte interface and how it can be used to measure a photocurrent of a particular sample. I will now discuss how to measure the EQE spectrum using a photoelectrochemical cell.

To determine an EQE of a sample, we simply measure the photocurrent produced at different photon energies and calibrate the data to the photocurrent produced by a standardised photodetector, which has a known EQE spectrum. The photocurrent, $\Delta J(E)$, of a sample and the photodiode is measured across a small range of photon energies, ΔE and subjected to an illumination with a spectral flux density, $b(E)$, which can be used to calculate a Quantum Efficiency using the following relation:

$$\Phi(E) = \frac{\Delta J\,(E)}{qb(E).\Delta E} \quad \textbf{(E.B.17)}$$

where q is the electronic charge (+ or -). The spectral flux is dependent on the intensity of the illumination source, which will be consistent for the measurement of photocurrent of both

the sample and photodiode. Therefore, $b(E)$, is considered as a constant and the EQE spectrum of the sample can therefore be calculated from the ratio of photocurrents between the sample and photodiode, multiplied by the EQE spectrum of the photo diode, using the following expression:

$$\Phi_S = \Phi_{pd} \frac{\Delta J_S}{\Delta J_{pd}} \quad \textbf{(E.B.18)}$$

Where each variable is a function of photon energy ($h\nu$) and the subscripts '*S*' and '*pd*' refer to the sample and the photodiode respectively.

To measure the photocurrent of a sample, the sample is placed in electrolytic cell described above. The electrolyte is made up of 0.1 M $NaSO_3$ and is contained in a glass cell for SnS_2 samples ($Eu^{2+/3+}$ for SnS samples). The electrolytic cell or photodetector are placed in a dark faraday box and illuminated using a monochromatic beam of light, which has been focused to a size smaller than the sample or photodetector. This means the photon flux is consistent for all measurements. During the measurements a potential stat is used to hold the sample under a fixed potential in order to produce the preferred band bending conditions. The potential is measured with respect to the reference electrode using a DC offset potentiostat. The photocurrent, recorded by the potentiostat, flows between the sample and the platinum counter electrode. In order to identify photocurrent from the dark current (a result of processes other than light absorption from the illumination source), the light beam is chopped at a consistent frequency and a lock-in amplifier is used to detect the modulated photocurrent at the same frequency. To provide the minimal reflection and absorption losses from the glass cell and electrolyte the sample surface is brought c.a. 1 mm from the edge of the cell wall facing the beam of light.

Calculating the predicted current density from EQE spectra

The EQE spectrum determines the percentage of photoelectrons generated from the incident photon flux. The percentage of photo generated current that be produced across a wide range of photon energies can be used to predict the short circuit current density, J_{sc}, that would be produced from the sample under a given illumination source.[27]

This prediction can be calculated by integrating the EQE spectrum multiplied by spectral photon flux density ($m^{-2}s^{-1}eV^{-1}$), $b(E)$, of an illumination source, as shown below:

$$J_{sc} = q\int_0^{\infty} \Phi(E)b(E)dE \quad \textbf{(E.B.19)}$$

Where q is the electronic charge. By substituting, $b(E)$, for the spectral photon flux density of the AM 1.5 G spectrum (the standardised solar photon flux for the Earth's surface), we can predict the J_{sc} for a sample if used within a fabricated device. The J_{sc} produced by a sample can be used to assess the film quality. A higher J_{sc} will improve a working device performance and indicates that the film can generate large number photo electrons with lower recombination rates. A comparative study of film quality can only be viable if the films have the same band gap. The band gap determines the lowest photon energy that can be absorbed by a material, which means that a material with a wider band gap energy will absorb a smaller number of photons and resulting a lower current density.

Measuring the flat-band potential (E_{fb}), the donor (N_d) or acceptor (N_a) density and potential dependant space charge region (W)

The flat-band potential, E_{fb}, is the potential at which the sample Fermi energy does not induce band bending at the semiconductor-electrolyte interface. At this potential it is expected that the degree of band bending, $\Delta\phi = 0$ and thus the space charge region, $W = 0$. Controlling the potential applied to the sample, E, we can control the width of the space charge region, W. Therefore we re-write the Gärtner equation by substituting the expression for W (**Equation E.B.20**) we can measure variation in quantum efficiency at different applied potential to calculate the E_{fp} of a sample:

$$-\ln(1-\Phi) = \alpha\frac{(2\varepsilon_0\varepsilon_r(E_{fb}-E))^{1/2}}{qN_{a|d}} \quad \textbf{(E.B.20)}$$

This equation is valid when $E<E_{fb}$, for a p-type semiconductor and $E>E_{fb}$ for an n-type semiconductor, in all other cases $\phi = 0$. Furthermore the illumination of the sample should be at a photon energy within 1 eV of the band gap energy to stay within the parabolic region of the absorption spectrum. Subsequently since $W = 0$ at the flat band potential the amount of photocurrent generated will be little or nothing, as the only driving force for carrier collection is diffusion and there is no longer an electric field to promote photo-electron-hole separation at the sample surface

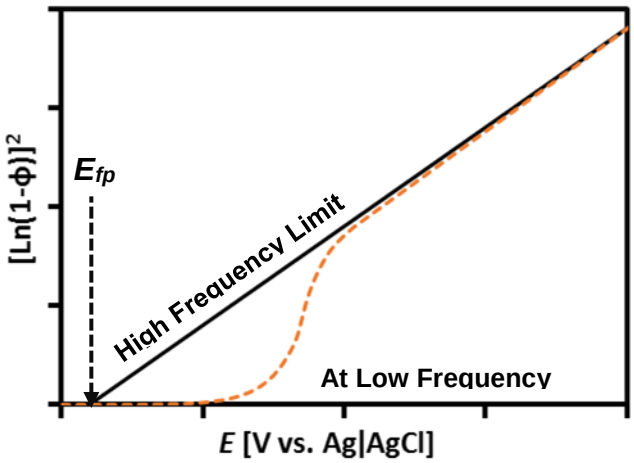

Figure B.45: EQE vs. Potential plot to determine the flat band potential, E_{fp}, illustrating the effect of surface recombination. High frequency illumination during measurements can eliminate the recombination effect and extend the linear region of the plot.

For an n-type material where, $E<E_{fb}$, electron begin to populate surface states and for a p-type material, where $E>E_{fp}$, a surface potential barrier is formed, in both cases, respectively, minority carriers are prevented from diffusing to the surface and react with the redox electrolyte. However, in the situation where $E<E_{fp}$, or $E>E_{fp}$ for a p-type or n-type semiconductor respectively, as the different between E and E_{fp} increases the space charge region will become large. In principle, according to equation **E.B.20**, a plot of [ln(1-ϕ)]2 against E should afford a straight line with an intercept at the x-axis equal to the E_{fp}. In practice this is not always observed. As the applied potential approaches zero, the space charge region becomes very small, subsequently recombination of photo generated electron-holes increases, since there is a smaller driving force for carrier separation and minority and majority carriers can recombine at a higher rate as they become temporarily trapped in surface states. Therefore at potentials close to the flat band potential the EQE (ϕ) is less than predicted from equation **E.B.20**, as illustrated in Figure 1.45, which can lead to E_{fp} being underestimated. There are two solutions to this problem. One solution is to extrapolate the linear region of the plot at higher potential, where the space charge region is large enough that the photocurrent losses are no longer significant. The second solution is to conduct the EQE measurements under high chopped illumination frequencies so that the photocurrent measurements are made on a time scale shorter than that of the recombination reaction.[28] It the plot of the EQE vs. potential is acceptable and produces a visible liner region, the flat band potential, E_{fp} and majority carrier densities, N_a/d can be derived from the data using equation **E.B.20** Furthermore the potential dependant space charge region, W, can also be derived from equation **E.B.15**.

References:

1. P. S. Ong, *X-Ray Spectrometry*, 1975, **4**, p 421.
2. D. Bell and A. Garratt-Reed, *Energy Dispersive X-ray Analysis in the Electron Microscope*, Taylor & Francis, 2003.
3. N. Fairley, C. S. Ltd and C. S. L. Staff, *CasaXPS Manual 2.3.15: Introduction to XPS and AES*, Casa Software, Limited, 2009.
4. R. E. Dinnebier and S. J. L. Billinge, in *Powder Diffraction: Theory and Practice*, The Royal Society of Chemistry, 2008, pp. 1-19.
5. G. Haugstad, in *Atomic Force Microscopy*, John Wiley & Sons, Inc., 2012, pp. 1-32.
6. P. Vandenabeele, in *Practical Raman Spectroscopy – An Introduction*, John Wiley & Sons, Ltd, 2013, pp. 1-38.
7. P. Vandenabeele, in *Practical Raman Spectroscopy – An Introduction*, John Wiley & Sons, Ltd, 2013, pp. 101-148.
8. T. Wildsmith, M. S. Hill, A. L. Johnson, A. J. Kingsley and K. C. Molloy, *Chemical Communications*, 2013, **49**, 8773-8775.
9. J. F. Scott, *The Journal of Chemical Physics*, 1970, **53**, 852-853.
10. H. R. Chandrasekhar, R. G. Humphreys, U. Zwick and M. Cardona, *Physical Review B*, 1977, **15**, 2177-2183.
11. I. Y. Ahmet, M. S. Hill, A. L. Johnson and L. M. Peter, *Chemistry of Materials*, 2015, **27**, 7680-7688.
12. R. E. Abutbul, E. Segev, L. Zeiri, V. Ezersky, G. Makov and Y. Golan, *RSC Advances*, 2016, **6**, 5848-5855.
13. M. Steichen, R. Djemour, L. Gütay, J. Guillot, S. Siebentritt and P. J. Dale, *The Journal of Physical Chemistry C*, 2013, **117**, 4383-4393.
14. D. G. Mead and J. C. Irwin, *Solid State Communications*, 1976, **20**, 885-887.
15. R. E. Abutbul, E. Segev, S. Samuha, L. Zeiri, V. Ezersky, G. Makov and Y. Golan, *CrystEngComm*, 2016, **18**, 1918-1923.
16. A. S. Pine and G. Dresselhaus, *Physical Review B*, 1971, **4**, 356-371.
17. A. C. Ferrari, J. C. Meyer, V. Scardaci, C. Casiraghi, M. Lazzeri, F. Mauri, S. Piscanec, D. Jiang, K. S. Novoselov, S. Roth and A. K. Geim, *Physical Review Letters*, 2006, **97**, 187401.
18. L. Bergman and J. L. McHale, *Handbook of Luminescent Semiconductor Materials*, Taylor & Francis, 2011.
19. F. A. Jenkins and H. E. White, *Fundamentals of Optics*, McGraw-Hill, 1976.
20. J. C. Manifacier, J. Gasiot and J. P. Fillard, *Journal of Physics E: Scientific Instruments*, 1976, **9**, 1002.
21. R. Swanepoel, *Journal of Physics E: Scientific Instruments*, 1983, **16**, 1214.
22. J. Tauc, *Materials Research Bulletin*, 1968, **3**, 37-46.
23. W. Schmickler and E. Santos, in *Interfacial Electrochemistry*, Springer Berlin Heidelberg, Berlin, Heidelberg, 2010, pp. 117-131.
24. in *Non-Tetrahedrally Bonded Elements and Binary Compounds I*, eds. O. Madelung, U. Rössler and M. Schulz, Springer Berlin Heidelberg, Berlin, Heidelberg, 1998, pp. 1-5.
25. S. Acharya and O. N. Srivastava, *physica status solidi (a)*, 1979, **56**, K1-K4.
26. R. Bacewicz, B. Pałosz, W. Pałosz and S. Gierlotka, *Solid State Communications*, 1985, **54**, 283-285.
27. J. Nelson, *The Physics of Solar Cells*, Imperial College Press, London, 2003.
28. R. Peat and L. M. Peter, *Applied Physics Letters*, 1987, **51**, 328-330.